PHYSICAL REVIEW E **89**, 021002(R) (2014)

Globally aligned states and hydrodynamic traffic jams in confined suspensions of active asymmetric particles

Adrien Lefauve and David Saintillan*

Department of Mechanical Science and Engineering, University of Illinois at Urbana-Champaign, Urbana, Illinois 61801, USA

(Received 24 July 2013; published 19 February 2014)

Strongly confined active liquids are subject to unique hydrodynamic interactions due to momentum screening and lubricated friction by the confining walls. Using numerical simulations, we demonstrate that two-dimensional dilute suspensions of fore-aft asymmetric polar swimmers in a Hele-Shaw geometry can exhibit a rich variety of novel phase behaviors depending on particle shape, including coherent polarized density waves with global alignment, persistent counterrotating vortices, density shocks and rarefaction waves. We also explain these phenomena using a linear stability analysis and a nonlinear traffic flow model, both derived from a mean-field kinetic theory.

DOI: 10.1103/PhysRevE.89.021002 PACS number(s): 47.57.E−, 87.18.Hf, 05.65.+b, 47.63.Gd

The spontaneous emergence of collective motion, large-scale coherent patterns, and complex unsteady flows is a generic feature of a wide variety of soft active systems [1–3], including bacterial swarms and suspensions [4–6], reactive and driven colloidal suspensions [7–9], cytoplasmic extracts [10], solutions of biological filaments and motor proteins [11,12], and shaken granular materials [13,14]. In these systems an immersed microstructure (such as self-propelled particles or biofilament–motor-protein assemblies) converts a source of energy (often chemical) into microstructural changes that create active stresses and can drive coherent flows on mesoscopic length scales. Analyzing how the interactions between individual agents translate into collective dynamics in these dissipative nonequilibrium systems has been the subject of intense research in the past few years and could pave the way for a deeper understanding of intracellular processes [15] and enable new paradigms for the design of smart materials [16–18] and autonomous micromachines [19–21].

The prototypical case of a collection of motile particles in a viscous liquid has received much scrutiny. Experiments on bulk microbial suspensions show that above a critical concentration spatiotemporally chaotic flows reminiscent of turbulence spontaneously arise [5] and are accompanied by a transition to local orientational order [4]. As demonstrated by particle simulations [22,23] and kinetic theories [24–26], this transition can in some cases be explained as a result of long-ranged hydrodynamic interactions (HIs) between swimmers, which are driven by the force dipoles exerted by the particles on the medium owing to self-propulsion [27]. These interactions drive a generic long-wave instability for the nematic order parameter in the form of bend modes in suspensions of rear-actuated swimmers [26]. Recent evidence suggests that direct steric interactions also play a role in dense systems [4,5,28].

The nature of HI between self-propelled particles, however, changes drastically under confinement (see, e.g., Ref. [29]). As a swimmer moves in a rigidly confined space, say, in the thin gap h between two parallel flat plates, the disturbance flow induced by its permanent force dipole is partially screened by the walls and decays rapidly as $\sim 1/r^3$ in the far field [30–32], where r is the distance from the particle, as opposed to the usual $1/r^2$ decay in the absence of confinement. Under these conditions, the far-field flow assumes the Hele-Shaw form and can be modeled as a two-dimensional (2D) potential flow [31]: $\mathbf{u}(\mathbf{r}) = -(h^2/12\eta)\nabla\Pi(\mathbf{r})$, where $\mathbf{r} = (x,y)$, η is the dynamic viscosity, and $\{\mathbf{u},\Pi\}$ denote the gap-averaged velocity and pressure fields. As a particle with thickness $\lesssim h$ located at position $\mathbf{R}(t)$ moves in an external flow $\mathbf{u}(\mathbf{r},t)$ in such a geometry, the disturbance velocity it induces is now dominated by a mass dipole singularity with $1/r^2$ spatial decay resulting from the displacement of the fluid by the finite volume of the particle [32,33]:

$$\mathbf{u}^d(\mathbf{r}|\mathbf{R}(t),\boldsymbol{\sigma}) = \frac{1}{2\pi|\mathbf{r}|^2}(2\hat{\mathbf{r}}\hat{\mathbf{r}} - \mathbf{I})\cdot\boldsymbol{\sigma}, \tag{1}$$

where $\mathbf{r}$ points from the particle center-of-mass $\mathbf{R}(t)$ and $\hat{\mathbf{r}} = \mathbf{r}/r$. The dipole strength is proportional to the relative velocity between the particle and background flow: $\boldsymbol{\sigma} = \sigma\{\dot{\mathbf{R}}(t) - \mathbf{u}[\mathbf{R}(t)]\}$, where the prefactor σ scales as the particle surface area in the (x,y) plane. Another defining feature of strongly confined systems is the way particles respond to a prescribed flow field. Brotto *et al.* [32] recently explained that an anisotropic swimmer lacking fore-aft symmetry (as is the case of most flagellated motile microorganisms) and undergoing lubricated friction with the walls will generally be subject to an anisotropic mobility and to alignment in both the flow and flow-gradient directions. Using a simple dumbbell model, they showed that the motion of a swimmer with position $\mathbf{R}$ and director $\mathbf{p}$ ($|\mathbf{p}| = 1$) in a flow field $\mathbf{u}$ obeys

$$\dot{\mathbf{R}} = v_s\,\mathbf{p} + \mu_\perp(\mathbf{I} - \mathbf{pp})\cdot\mathbf{u} + \mu_\parallel\,\mathbf{pp}\cdot\mathbf{u}, \tag{2}$$

$$\dot{\mathbf{p}} = \nu(\mathbf{I} - \mathbf{pp})\cdot\mathbf{u} + \nu'(\mathbf{I} - \mathbf{pp})\cdot\nabla\mathbf{u}\cdot\mathbf{p}. \tag{3}$$

Here v_s is the swimming speed, and $\mu_{\perp,\parallel}$ are the transverse and longitudinal mobilities. While reorientation by the flow gradient (with constant ν') corresponds to the well-known Jeffery's equation, reorientation by the velocity itself is a consequence of confinement and fore-aft asymmetry, with "large-head" swimmers ($\nu < 0$) aligning against the flow and

*Present address: Department of Mechanical and Aerospace Engineering, University of California San Diego, La Jolla, CA 92093, USA; dstn@ucsd.edu

"large-tail" swimmers ($\nu > 0$) with the flow [32]. On very large length scales, reorientation by the velocity is in fact expected to be the dominant mechanism for particle alignment, as the corresponding angular flux scales with $\mathbf{u}$ itself rather than its gradient. Based on these effects, Brotto *et al*. derived a kinetic model for a 2D suspension of interacting confined swimmers and predicted a novel long-wave linear instability of the homogeneous isotropic phase, amplifying perturbations in longitudinal polarization. However, the phase behavior and pattern formation that these instabilities lead to in the nonlinear regime in finite-sized systems remain unknown.

This Rapid Communication presents a detailed description of these nonlinear dynamics via discrete particle simulations and mean-field kinetic models of rigidly confined 2D suspensions. We show that the distinctive features of HI and asymmetric swimmer orientational dynamics under confinement lead to a rich variety of phase behaviors unobserved in unconfined bulk systems. We first describe the spontaneous emergence of coherent polarized density waves and of persistent counterrotating vortices from the isotropic phase. The presence of density shocks and rarefaction waves in a narrow channel with background flow is then elucidated, and their novel character genuinely pertaining to active propulsion is emphasized.

We simulate the 2D dynamics of a large number N of confined point particles by integrating (2)-(3) in time, where the velocity $\mathbf{u}$ is the superposition of the dipolar fields driven by the swimmers according to (1). We also impose rotational diffusion with diffusivity d by adding to $\dot{\mathbf{p}}$ a vector $\sqrt{2d/\delta t}\,(\mathbf{I}-\mathbf{pp})\cdot\mathbf{n}$, where δt is the time step and the components of $\mathbf{n}$ follow a normal distribution with zero mean and unit variance. Center-of-mass diffusion is not imposed, though the coupling between rotational diffusion and swimming naturally introduces spatial diffusion, with long-time diffusivity $D = v_s^2/2d$ in the isotropic phase [34]. The computational domain is a 2D square box of linear size L, and particle positions and orientations are initialized randomly following a uniform law. Dipolar interactions between particles and their periodic images are computed accurately using an efficient algorithm [35]. We scale time by the orientational relaxation time scale d^{-1} and lengths by the distance $\ell = v_s/2d$ traveled by a swimmer before it loses memory of its orientation. We set $\mu_{\perp,\parallel} = 1$, $\nu' = 0$, and focus primarily on the influence of the polar alignment parameter ν and system size L/ℓ, as well as area fraction $\phi = \sigma c_0/2$ (with $c_0 = N/L^2$ the number density). Following Brotto *et al*. and anticipating our results, we introduce a signed Péclet number $\mathrm{Pe} = 2\nu\phi\ell$ comparing the rotation rate of a swimmer by the dipolar flows induced in the suspension and by rotational diffusion, and we recall that long-wave polarization fluctuations are predicted to be unstable for large-head swimmers when $\mathrm{Pe} < -1$ [32].

A typical simulation in this regime is shown in Fig. 1 and online video [35] for $N = 5000$, $\phi = 1\%$, and $\mathrm{Pe} = -2.2$. Starting from uniform isotropy, Fig. 1(a) shows heavily polarized sharp density waves, which travel in arbitrary directions and exhibit a distinct curvature indicative of splay. The formation and growth of these waves is clearly seen on a spatiotemporal diagram of the longitudinal concentration in Fig. 1(b), where swimmers are found to concentrate on a sharp front propagating at a characteristic speed $\approx 0.7 v_s$. To

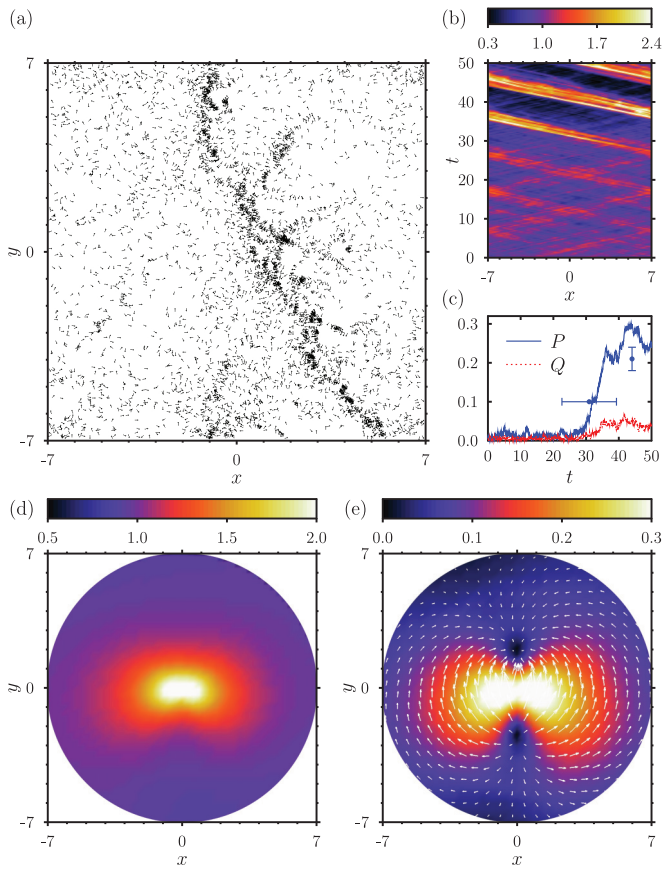

FIG. 1. (Color online) Direct simulation with $N = 5000$, $L/\ell = 14$, $\phi = 1\%$, and $\mathrm{Pe} = -2.2$. (a) Snapshot of the polarized density waves. (b) Spatiotemporal diagram of longitudinal concentration. (c) Global polar and nematic order parameters. Error bars show one standard deviation for the transition time and plateau value of P over 10 simulations. (d) Pair distribution function $g(\mathbf{r})$. (e) Pair polarization $\mathbf{P}(\mathbf{r})$, with colors indicating $|\mathbf{P}|$.

quantify particle alignment, we define a global polar order parameter $P = |\langle\mathbf{p}\rangle|$ (where $\langle\cdot\rangle$ is the suspension average) and a global nematic order parameter Q as the positive eigenvalue of $\langle\mathbf{pp} - \mathbf{I}/2\rangle$. Both are shown in Fig. 1(c) to grow from zero as the instability develops and to plateau at long times when polarization appears to dominate. The emergence of global alignment is particularly surprising given the nonaligning nature of dipolar interactions. The structure of the density waves is further characterized in Fig. 1(d), showing the 2D pair distribution function $g(\mathbf{r})$ or probability of finding a second swimmer at position $\mathbf{r}$ if a first swimmer is located at the origin and points in the $+y$ direction. The anisotropy and curvature of the peak at the origin are consistent with the presence of longitudinal curved density waves. The pair polarization $\mathbf{P}(\mathbf{r})$ is also shown in Fig. 1(e) and has the symmetry of a potential dipole flow, with direction opposite that of the flow driven by the particle at the origin as expected for swimmers that align against the flow ($\nu < 0$).

To substantiate the observed pattern formation, we revisit the linear stability analysis of Brotto *et al*. [32] at finite wave number. The configuration of the suspension is described by the probability distribution $\Psi(\mathbf{r},\mathbf{p},t)$ of finding a particle at

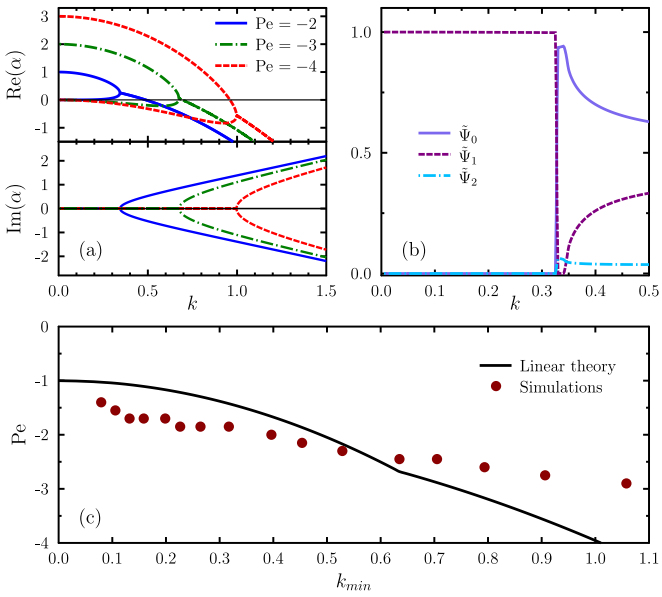

FIG. 2. (Color online) (a) Real and imaginary parts of the growth rate α vs k for various unstable values of Pe. (b) Harmonic content of the unstable modes: zeroth, first and second harmonics vs k for Pe $= -2$. (c) Marginal Péclet number for instability vs wave number, from theory and simulations. Error bars are of the order of the symbol size.

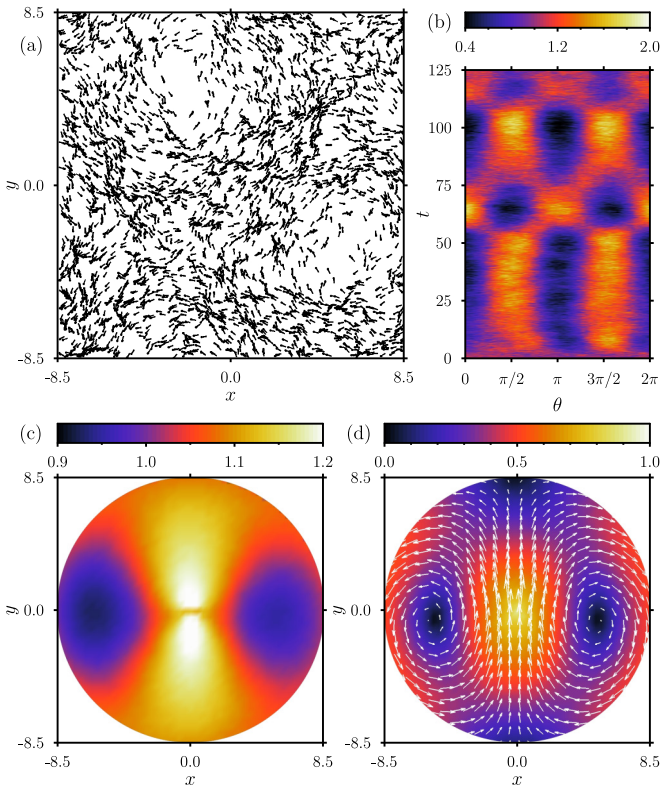

FIG. 3. (Color online) Direct simulation with $N = 3600$, $L/\ell = 17$, $\phi = 10\%$, and Pe $= 3.7$. (a) Snapshot of two counterrotating vortices. (b) Temporal diagram of the mean orientation distribution, where $\theta = \cos^{-1}(\mathbf{p}\cdot\hat{\mathbf{x}})$. (c) Pair distribution function $g(\mathbf{r})$. (d) Pair polarization $\mathbf{P}(\mathbf{r})$.

position $\mathbf{r}$ with orientation $\mathbf{p}$ at time t, which satisfies the Smoluchowski equation [24]

$$\partial_t \Psi + \nabla_r \cdot (\dot{\mathbf{R}}\Psi) + \nabla_p \cdot (\dot{\mathbf{p}}\Psi) = D\nabla_r^2\Psi + d\nabla_p^2\Psi, \qquad (4)$$

with $\dot{\mathbf{R}}$ and $\dot{\mathbf{p}}$ defined in (2)–(3), where the fluid velocity is now obtained as $\mathbf{u}(\mathbf{r},t) = \iint \Psi(\mathbf{r}',\mathbf{p},t)\mathbf{u}^d(\mathbf{r}|\mathbf{r}',\sigma)\,d\mathbf{r}'d\mathbf{p}$. We analyze the linear stability of the uniform isotropic state to a weak plane-wave perturbation with arbitrary wave vector $\mathbf{k}$: $\Psi(\mathbf{r},\mathbf{p},t) = c_0/2\pi + \varepsilon\tilde{\Psi}(\mathbf{p})\exp(i\mathbf{k}\cdot\mathbf{r} + \alpha t)$, where α is the complex growth rate and $|\varepsilon| \ll 1$. Linearization of (4) about this state yields an eigenvalue problem for $\{\alpha,\tilde{\Psi}\}$ that can be solved numerically. The dispersion relation $\alpha(k)$ is shown in Fig. 2(a), where a positive growth rate is seen to occur when Pe < -1 for sufficiently small wave numbers. In the limit of $k \to 0$, we recover the long-wave result of Brotto *et al.* [32]: Re$(\alpha) = -(1 + \text{Pe})$. The unstable eigenmodes are illustrated in Fig. 2(b), showing the zeroth, first, and second Fourier coefficients of $\tilde{\Psi}(\theta)$ where $\theta = \cos^{-1}(\mathbf{p}\cdot\hat{\mathbf{k}})$, corresponding to fluctuations in concentration, polar, and nematic splay alignments, respectively. At very low k, the instability pertains only to polarization in agreement with Brotto *et al.*, but if $-3 <$ Pe < -1 there also exists a finite range of wave numbers for which the unstable eigenmodes couple all three harmonics and propagate spatially as shown by the nonzero value of Im(α). This is consistent with the observations in Fig. 1 (Pe $= -2.2$, $k \geqslant 0.44$), and the ratio of $\tilde{\Psi}_1$ and $\tilde{\Psi}_2$ in Fig. 2(b) also mirrors that of P and Q in the nonlinear regime. A more quantitative comparison with the simulations is provided in Fig. 2(c), showing the marginal Péclet number for instability vs $k_{\min} = \sqrt{2}\pi\ell/L$, or the smallest wave number in a system of size L. Qualitative agreement is found, with some level of discrepancy, which we attribute to the discrete nature of the simulations, finite amplitude of the fluctuations in the initial random condition, and nonlinearities.

We now turn to suspensions of large-tail swimmers ($v > 0$), which, except at very high densities, are linearly stable [32]. However, our simulations still reveal unusual dynamics for sufficiently positive values of Pe. As shown in Fig. 3(a) and online video [35], these suspensions indeed tend to develop active "lanes," which often organize around pairs of large-scale counterrotating vortices. A strong nematic alignment exists at all scales including the system size, as evidenced by the mean orientation distribution in Fig. 3(b) exhibiting two peaks separated by π. In addition, the temporal evolution of the orientations suggests the presence of persistent stationary structures that quasiperiodically form and break up over long periods. The pair distribution function in Fig. 3(c) shows a characteristic stripe in the longitudinal direction consistent with the presence of lanes, and the pair polarization still has a dipolar symmetry, with $\mathbf{P}$ now expectedly pointing in the opposite direction to that previously observed for large-head swimmers. The emergence of such large-scale motions and global orientational order, which is not predicted by the linearized kinetic model, must arise from nonlinear interactions and has yet to be explained theoretically.

Complex dynamics have previously been reported in passive confined systems, and notably in driven emulsions under a uniform flow in a narrow Hele-Shaw cell [33,36], where the formation of density shocks was reported. To contrast the case of active particles to these driven systems,

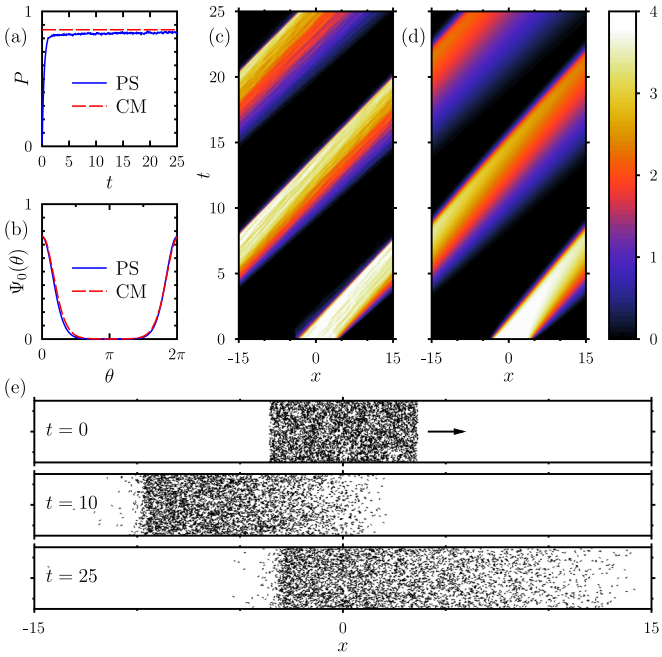

FIG. 4. (Color online) Density waves in a narrow channel with a uniform flow, with periodic boundary conditions along x. Comparison between particle simulation (PS) ($N = 4000$, $\phi = 0.05$, $\xi = 4$, $L \times W = 30\ell \times 3\ell$) and numerical solution of the continuum model (5) (CM). (a) Mean polarization P rapidly reaching P_0 (polar stable state). (b) Steady orientation distribution. (c)–(d) Spatiotemporal diagrams of longitudinal concentration from PS and CM, respectively. (e) Particle distributions (particles are magnified).

we also analyze the dynamics in a suspension of asymmetric swimmers confined in a narrow channel when a uniform external flow $\mathbf{U}_0 = U_0\hat{\mathbf{x}}$ is applied in the longitudinal direction (Fig. 4). A sufficiently strong flow can be shown to suppress the collective motions observed above by controlling the alignment of the fore-aft asymmetric swimmers. Orientations then approximately decouple from spatial concentration fluctuations, which become quasi-one-dimensional (1D): $\Psi(\mathbf{r},\mathbf{p},t) \approx c(x,t)\Psi_0(\theta,t)$, with $\theta = \cos^{-1}(\mathbf{p}\cdot\hat{\mathbf{x}})$. The steady anisotropic orientation distribution is easily obtained as $\Psi_0(\theta) = C\exp(\xi\cos\theta)$, where C is a normalization constant and $\xi = \nu U_0/d$ a dimensionless flow strength, with a net longitudinal polarization $P_0 = \int \Psi_0(\theta)\cos\theta\, d\theta \neq 0$ as indeed observed in simulations [Figs. 4(a)–4(b)]. Assuming the form of interactions is unchanged by the lateral boundaries in the y direction, the Smoluchowski equation (4) then simplifies to a 1D conservation equation for $c(x,t)$:

$$\partial_t c + \partial_x[U_0 c + v_s P_0(1-\sigma c)c] = D\partial_{xx}c, \tag{5}$$

where the only difference between large-head and large-tail swimmers appears in the sign of P_0. This quasilinear wave equation is commonly used as a basic model for traffic flow behavior [37,38], where the coefficient $v_s P_0(1-\sigma c)$ can be interpreted as an Eulerian concentration-dependent velocity. The mean single-swimmer x velocity $v_s P_0$ is renormalized by interactions: it is largest where $c(x) = 0$ and decays linearly with c to reach zero where $c(x) = 1/\sigma$, the maximum concentration. Wave solutions of (5) are characterized by the emergence of a shock at the rear and a rarefaction wave at the front, much like in a typical traffic jam. A shock and rarefaction wave are indeed observed in particle simulations in Figs. 4(c) and 4(e) and online video [35], showing the evolution of an initially uniform and isotropic finite-sized plug, and excellent agreement is found with a numerical solution of the traffic flow equation (5) in Fig. 4(d). In previous experiments on driven confined emulsions [33,36], density shocks also occurred, albeit at the front of the waves, and were explained as a consequence of interactions with lateral boundaries. While boundary interactions, which are taken into account in our simulations [35], still likely play a role in the present system, the primary mechanism here is the truly novel combined effect of active self-propulsion and renormalization by interparticle dipolar interactions.

We thank Denis Bartolo and Saverio Spagnolie for useful conversations and gratefully acknowledge funding from NSF CAREER Grant No. CBET-1150590.

[1] S. Ramaswamy, Annu. Rev. Condens. Matter **1**, 323 (2010).
[2] D. Saintillan and M. J. Shelley, C. R. Physique **14**, 497 (2013).
[3] M. C. Marchetti *et al.*, Rev. Mod. Phys. **85**, 1143 (2013).
[4] L. H. Cisneros, J. O. Kessler, S. Ganguly, and R. E. Goldstein, Phys. Rev. E **83**, 061907 (2011).
[5] J. Dunkel *et al.*, Phys. Rev. Lett. **110**, 228102 (2013).
[6] X. Chen, X. Dong, A. Be'er, H. L. Swinney, and H. P. Zhang, Phys. Rev. Lett. **108**, 148101 (2012).
[7] S. J. Ebbens and J. R. Howse, Soft Matter **6**, 726 (2010).
[8] D. Takagi, A. B. Braunschweig, J. Zhang, and M. J. Shelley, Phys. Rev. Lett. **110**, 038301 (2013).
[9] A. Bricard, J.-B. Caussin, N. Desreumaux, O. Dauchot, and D. Bartolo, Nature (London) **503**, 95 (2013).
[10] F. G. Woodhouse and R. E. Goldstein, Phys. Rev. Lett. **109**, 168105 (2012).
[11] V. Schaller, C. Weber, C. Semmrich, E. Frey, and A. Bausch, Nature (London) **467**, 73 (2010).
[12] T. Sanchez, D. T. N. Chen, S. J. DeCamp, M. Heymann, and Z. Dogic, Nature (London) **491**, 431 (2012).
[13] A. Kudrolli, G. Lumay, D. Volfson, and L. S. Tsimring, Phys. Rev. Lett. **100**, 058001 (2008).
[14] J. Deseigne, O. Dauchot, and H. Chaté, Phys. Rev. Lett. **105**, 098001 (2010).
[15] F. G. Woodhouse and R. E. Goldstein, Proc. Natl. Acad. Sci. USA **110**, 14132 (2013).
[16] Y. Hatwalne, S. Ramaswamy, M. Rao, and R. A. Simha, Phys. Rev. Lett. **92**, 118101 (2004).
[17] R. Voituriez, J.-F. Joanny, and J. Prost, Europhys. Lett. **70**, 404 (2005).
[18] L. Giomi, L. Mahadevan, B. Chakraborty, and M. F. Hagan, Phys. Rev. Lett. **106**, 218101 (2011).

[19] N. Darnton, L. Turner, K. Breuer, and H. C. Berg, Biophys. J. **86**, 1863 (2004).
[20] A. Sokolov, M. M. Apodaca, B. A. Grzybowski, and I. S. Aranson, Proc. Natl. Acad. Sci. USA **107**, 969 (2010).
[21] R. Di Leonardo *et al*., Proc. Natl. Acad. Sci. USA **107**, 9541 (2010).
[22] J. P. Hernandez-Ortiz, C. G. Stoltz, and M. D. Graham, Phys. Rev. Lett. **95**, 204501 (2005).
[23] D. Saintillan and M. J. Shelley, Phys. Rev. Lett. **99**, 058102 (2007); J. R. Soc. Interface **9**, 571 (2012).
[24] D. Saintillan and M. J. Shelley, Phys. Rev. Lett. **100**, 178103 (2008); Phys. Fluids **20**, 123304 (2008).
[25] G. Subramanian and D. L. Koch, J. Fluid Mech. **632**, 359 (2009).
[26] A. Baskaran and M. C. Marchetti, Proc. Natl. Acad. Sci. USA **106**, 15567 (2009).
[27] K. Drescher, J. Dunkel, L. H. Cisneros, S. Ganguly, and R. E. Goldstein, Proc. Natl. Acad. Sci. USA **108**, 10940 (2011).
[28] B. Ezhilan, M. J. Shelley, and D. Saintillan, Phys. Fluids **25**, 070607 (2013).
[29] H. Wioland, F. G. Woodhouse, J. Dunkel, J. O. Kessler, and R. E. Goldstein, Phys. Rev. Lett. **110**, 268102 (2013).
[30] N. Liron and S. Mochon, J. Eng. Math. **10**, 287 (1976).
[31] S. Bhattacharya, J. Bławzdziewicz, and E. Wajnryb, J. Comp. Phys. **212**, 718 (2006).
[32] T. Brotto, J.-B. Caussin, E. Lauga, and D. Bartolo, Phys. Rev. Lett. **110**, 038101 (2013).
[33] T. Beatus, T. Tlusty, and R. Bar-Ziv, Phys. Rev. Lett. **103**, 114502 (2009); T. Beatus, R. H. Bar-Ziv, and T. Tlusty, Phys. Rep. **516**, 103 (2012).
[34] H. C. Berg, *Random Walks in Biology* (Princeton University Press, Princeton, 1993).
[35] See Supplemental Material at http://link.aps.org/supplemental/10.1103/PhysRevE.89.021002 for a description of the numerical methods and for videos illustrating the dynamics of Figs. 1, 3, and 4.
[36] N. Desreumaux, J.-B. Caussin, R. Jeanneret, E. Lauga, and D. Bartolo, Phys. Rev. Lett. **111**, 118301 (2013).
[37] G. B. Whitham, *Linear and Nonlinear Waves* (Wiley, New York, 1974).
[38] T. Nagatani, Rep. Prog. Phys. **65**, 1331 (2002).